POAC'23
Glasgow, United Kingdom

Proceedings of the 27th International Conference on
Port and Ocean Engineering under Arctic Conditions
12-16 June 2023, Glasgow, United Kingdom

On the dependency of the development of frequency lock-in on the mode shape amplitude for higher structural modes

Tim C. Hammer[1*], Hayo Hendrikse[1]

[1] Delft University of Technology, Department of Hydraulic Engineering, Delft, The Netherlands

ABSTRACT

Drifting sea ice failing in crushing against vertically-sided offshore structures can cause ice-induced vibrations. Offshore structures are typically founded on slender structures to minimize the load effect of waves and currents. In combination with large top masses, those offshore structures often provide sufficient compliance for ice-induced vibrations to develop. Although modern offshore structures can be expected to experience ice-induced vibrations in higher structural modes, this phenomenon is rarely considered during experiments and numerical analysis of dynamic ice-structure interaction. Inspired by this challenge, we investigated experimentally how the *sole* change of mode shape amplitude relation between higher structural modes at the water level of a multi-degree-of-freedom structure influences the development of frequency lock-in. Experiments of four different multi-degree-of-freedom structures in cold model ice have been performed in Aalto Ice and Wave Tank. To allow full control over the eigensystem during testing, modal representations of structures were implemented in the numerical domain of a hybrid test setup. When changing the mode shape amplitude, the total structural stiffness at the ice action point and modal damping as a fraction of critical were kept constant between the four structures. We found that the structure experienced sustained frequency lock-in vibrations in a frequency corresponding to the mode shape amplitude of artificially high magnitude. When mode shape amplitudes of two eigenmodes were equalized, the structure experienced oscillations in the frequency of the mode with lower frequency or lower damping mainly. It was found that ice-induced vibrations of multi-degree-of-freedom structures are highly dependent on the relative velocity between the ice and structure and thus on the superposition of higher mode oscillations with lower mode oscillations.

KEY WORDS

Model testing; Multi-modal vibrations; Frequency lock-in; Hybrid test setup

INTRODUCTION

Flexible bottom-founded structures—such as offshore wind turbines, lighthouses, channel markers, and offshore platforms—can, depending on the ice drift speed, ice thickness, and other factors, be expected to experience ice-induced vibrations when interacting with sea ice. Such ice-induced vibrations are subclassified as intermittent crushing, frequency lock-in and

continuous brittle crushing for a structure with a single dominant mode at the ice action point (Sodhi, 2001). Dominant modes herein are defined as modes with a high amplitude at the point of ice action, nominally at the water level. Structures with multiple modes of comparable amplitude at the ice action point, e.g. offshore wind turbines, have been shown experimentally to experience multi-modal interaction with ice (Hammer et al., 2023). During frequency lock-in, the structure motion is characterized by a quasi-harmonic oscillation. For a single-degree-of-freedom structure, the frequency of the oscillation is close to the only existent (first) eigenfrequency. However, a multi-degree-of-freedom structure does not necessarily oscillate close to the first eigenfrequency during frequency lock-in. As one example, offshore wind turbines showed oscillations with a frequency close to the second eigenfrequency when tested in model ice (Hammer et al., 2023). Multi-modal interaction occurs at low ice drift speeds (between intermittent crushing and frequency lock-in) and can be characterized by a periodic amplified first mode response, where in the interval when the ice and structure on average move against each other, the first mode response is superposed with oscillations of a frequency close to the first, second, and rarely third structural eigenmode (Hammer et al., 2022).

First experiments to investigate the influence of structural properties on the dominant mode during ice-induced vibrations were performed by Määttänen (1983). The author found that the structure would vibrate in the lowest natural mode until the velocity became too high for the first mode to follow. Other small-scale experiments of a cylindrical structure in model ice confirmed that steady-state vibrations would occur at the lowest natural frequency (Kärnä et al., 2003). Further small-scale experiments were conducted by Määttänen et al. (2012) to analyze the effect of excitation of multiple structural modes on the magnitude of identified forces during ice-induced vibrations. From that data, Nord et al. (2013) found that the maximum ice force occurred when multiple structural frequencies were activated. Extending this finding, Nord et al. (2015) showed that the transition velocity, at which the structural response shifted from first to second mode oscillations, increased with reduced structural stiffness and reduced superstructure mass. However, once the setup stiffness was changed by adjusting clamps, so was the natural frequency, which is why the conclusion of Nord et al. (2015) should rather be that the second mode oscillation increased with a reduced structural stiffness, reduced superstructure mass, *and reduced structural frequency*. A similar comment was already given by Hendrikse and Nord (2019) when analyzing the experimental tests of Huang et al. (2007), which shows the challenge of isolating single parameters for sensitivity analysis during basin experiments.

Besides these tests specifically aimed at investigating frequency lock-in, there are also more general challenges which make it difficult to study dynamic ice-structure interaction in small scale. Due to the commonly chosen scaling approach (Cauchy and Froude), only the first two structural modes can typically be investigated, as limited by capacity of the test facilities. Moving a (carriage) indenter into the ice, it can be challenging to keep a constant velocity at low velocities (Määttänen, 1983), interfering with the interaction process. Scaling of ice will also affect the observed failure modes. Although crushing ice was attempted to be tested, buckling failure (Tian et al, 2019), or mixed crushing and bending ice failure occurred when structures in model ice had been investigated in the past (Barker et al., 2005; Hendrikse et al., 2018).

Inspired by these challenges, we investigated experimentally how the *sole* change of mode shape amplitude relation between higher structural modes at the water level of a multi-degree-of-freedom structure with low natural frequencies influences the development of mode vibration during ice-structure interaction, typically referred to as frequency lock-in.

TEST SETUP

To answer our research question, it was of greatest importance to keep the ice failure mode, the carriage velocity in the ice tank, and structural properties of total stiffness, modal eigenfrequencies, and damping constant while having full control over the mode shape amplitudes. To achieve that, real-time hybrid experiments of a vertical, cylindrical aluminum pile in model ice were performed in the Aalto Ice and Wave Tank (Hendrikse et al., 2022a) as shown in Figure 1. A real-time hybrid experiment is a hybrid combination of a numerical solver and a physical measurement component. In our case, we measured the ice force on a rigid pile as it was dragged through model ice. The measured ice forces $F_{ice}(t)$ were used in a numerical solver in real time to solve for the modal displacement $w_i(t)$ of mode *i* at time *t*:

$$\ddot{w}_i(t) + 2 \cdot \zeta_i \cdot \omega_i \cdot \dot{w}_i(t) + \omega_i^2 \cdot w_i(t) = \phi_i^* \cdot F_{ice}(t) \qquad [\text{N kg}^{-0.5}] \qquad (1))$$

, where an overdot represents the derivative with respect to time, ω_i is the natural frequency of mode i, and ζ_i the damping ratio as a fraction of critical. The modal amplitude at the ice action point was represented by a mass normalized value ϕ_i^*, so that $\boldsymbol{\phi}^{*T} \cdot \boldsymbol{M} \cdot \boldsymbol{\phi}^* = \boldsymbol{I}$. The modal displacements were transferred into the structural displacement per actuator axis, d_x and d_y and then forwarded to the controller of the electrical actuators which controlled the motion of the cylindrical aluminum pile. For more information about the measurement equipment, the reader is referred to Hammer et al. (2021).

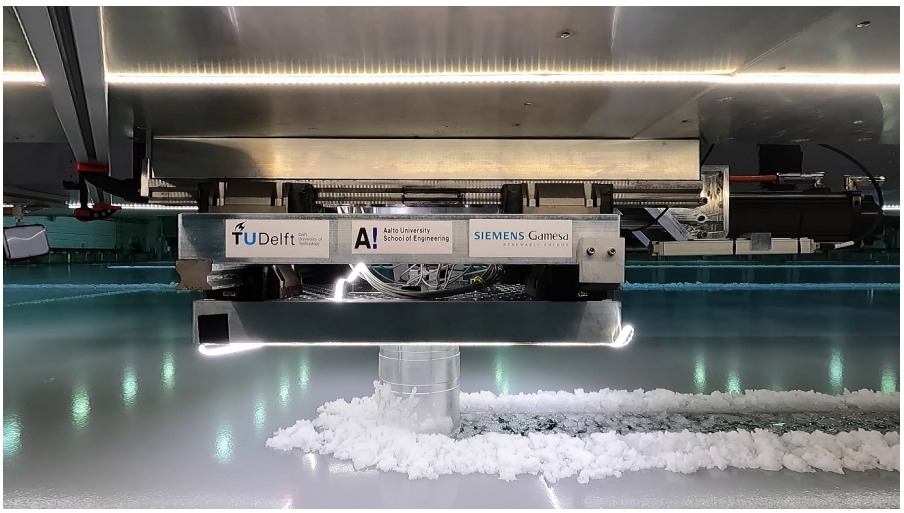

Figure 1. Side view of the hybrid test setup during experiments in the Aalto Ice and Wave Tank.

As we were interested in ice-induced vibrations caused by crushing level ice (insignificant gravity effects), we did not apply Froude scaling. Once Froude scaling was rejected, Cauchy scaling no longer required a reduction in ice strength (Palmer and Dempsey, 2009). We therefore aimed to test cold model ice which would fail in crushing. As we assumed that the phenomenon of ice-structure interaction may be driven by processes occurring at the microscopic scale (e.g. Cole (2021)), the geometric scaling was relaxed. The only scaling factor applied was based on a comparison of a simulated brittle crushing mean load in full scale to values measured during continuous brittle crushing tests in the cold model ice. See Hammer & Hendrikse (2023) for more detail on this approach applied to an offshore wind turbine. For the current study, scaling does not play a big role as we did not target any specific structure.

EIGENSYSTEM SCALING

As a hybrid test setup allows full control over the structural properties, we numerically tuned the specific mass-normalized mode shapes, while keeping the tuned total structural stiffness k_{tuned} equal to the original total structural waterline stiffness k_{total}:

$$k_{total} = \left(\sum_{i=1}^{n} \frac{\phi_i^{*2}}{4 \cdot \pi^2 \cdot {f_i}^2} \right)^{-1} = k_{tuned} \qquad [\mathrm{N\ m^{-1}}] \qquad (2)$$

Where f_i is the structural frequency per mode *i*. Using equation (2), we scaled structural properties of four different configurations, which are summarized in Table 1.

Table 1. Overview of structures considered in the present study.

			Case 1	**Case 2**	**Case 3**	**Case 4**
Structural mode $\boldsymbol{i}$	f_i	ζ_i	$\boldsymbol{\Phi}^*_{y,ref}$	$\boldsymbol{\Phi}^*_{y,eq}$	$\boldsymbol{\Phi}^*_{y,23}$	$\boldsymbol{\Phi}^*_{y,32}$
	[Hz]	[%]	[10^{-3} $kg^{-0.5}$]	[10^{-3} $kg^{-0.5}$]	[10^{-3} $kg^{-0.5}$]	[10^{-3} $kg^{-0.5}$]
1	0.154	0.8	1.88	1.88	1.88	1.88
2	0.888	1.3	14.79	15.75	17.83	3.29
3	1.66	1.9	18.72	15.75	1.78	32.86
4	2.91	4.1	7.53	7.53	7.53	7.53

All configurations consisted of the first four global bending modes of a full structure. Structural frequencies and damping were constant over all configurations and were set by a reference configuration $\boldsymbol{\Phi}^*_{y,ref}$, which was based on an offshore wind turbine (Hammer et al., 2023). For the column of $\boldsymbol{\Phi}^*_{y,eq}$ we tuned the second and third global bending mode to be of equal magnitude; for the column of $\boldsymbol{\Phi}^*_{y,23}$ the second mode shape amplitude was a magnitude larger than for the third global bending mode; and for the column of $\boldsymbol{\Phi}^*_{y,32}$, it was vice versa. As one example, we show the tuning of the third mode shape amplitude for the scaled structure $\boldsymbol{\Phi}^*_{y,32}$:

$$\phi^*_{y,32,3} = \sqrt{\frac{{k_{total}}^{-1} - \frac{\phi_1^{*2}}{4 \cdot \pi^2 \cdot {f_1}^2} - \frac{\phi_4^{*2}}{4 \cdot \pi^2 \cdot {f_4}^2}}{\frac{0.01}{4 \cdot \pi^2 \cdot {f_2}^2} + \frac{1}{4 \cdot \pi^2 \cdot {f_3}^2}}} \qquad [\mathrm{kg^{-0.5}}] \qquad (3)$$

An overview of the conducted tests can be found in Table 2. Each structure was tested for four different ice drift speeds on the 23.06.2021. All tests were conducted within two runs of the same ice sheet at an ambient temperature T of -11°C. The compressive and flexural strength of the ice sheet (σ_c, σ_f) were tested according to International Towing Tank Conference procedures (2014). The ice thickness h was measured at four different locations along the tested channel and is given as a mean value in Table 2 next to an overview of the other test parameters.

Table 2. Overview of tests considered in the present study.

Case	Test ID	Ice drift speed	Test day and run	T	σ_c	σ_f	h
		[mm s^{-1}]		[°C]	[kPa]	[kPa]	[mm]
$\phi^*_{y,ref}$	604, 605, 606, 607	20, 30, 40, 50	23.06.2021 Run 6	-11°C	658	470	29
$\phi^*_{y,eq}$	608, 609, 610, 611	20, 30, 40, 50	23.06.2021 Run 6	-11°C	658	470	29
$\phi^*_{y,23}$	612, 613, 614, 615	20, 30, 40, 50	23.06.2021 Run 7	-11°C	658	470	31
$\phi^*_{y,32}$	616, 617, 618, 619	20, 30, 40, 50	23.06.2021 Run 7	-11°C	658	470	31

EXPERIMENTAL RESULTS

In this section, we analyze the results of measured structural displacements d_y, ice load F_y, and corresponding frequencies over time for each tested case separately. All results shown are based on experiments, in which we moved a vertical, aluminum pile, as part of a hybrid test setup, which was mounted to a carriage, through the ice. We refer to the tested, constant carriage speeds as ice drift speed in the following sections. We only show the last 50 seconds of the full time series (≈100 seconds) in the result sections to minimize the influence of transient vibrations on the results.

Case 1 - Reference structure

In the first case, we tested a reference structure consisting of the first four global bending modes of an offshore wind turbine. The full structural model had been used for experiments of offshore wind turbines in model ice (Hammer, Willems and Hendrikse, 2023). Experimental results (d_y, F_y) for an ice drift speed of 30 mm s^{-1} are shown in Figure 2. The measured structural displacement d_y shows that the tested structure experiences ice-induced vibrations. More specifically, the structural displacement shows mode contributions of at least three different modes.

Analyzing the time series in the frequency domain, we can quantify those structural modes. For better mode identification, the chosen grid illustrates the structural frequencies as listed in Table 1. Note that the resampling of the data results in a lower resolution of the frequency output and thus in small differences between structural frequencies in Table 1 and indicated frequencies in the figure. The results show that the structure, over the full test length, oscillated with a frequency slightly below the first eigenfrequency. Additionally, we see that the structure, especially in the beginning and in the end of the test, vibrated in a frequency below the second eigenfrequency. Next to oscillations of the second eigenfrequency, the structure experienced vibrations with oscillation slightly below the third eigenfrequency. It was observed that third mode vibrations mainly occurred or interfered with the development of sole second mode vibrations, once the structure and ice were moving on average in opposite directions, thus with increasing relative velocity (see Figure 3 left). The change in relative velocity seemed to induce the development of third mode vibration.

Focusing on the measured ice load F_y in Figure 2, we notice that single load peaks occurred once the structure experienced second mode oscillations. It is also interesting to observe that single instances exist when the measured ice load almost dropped to zero. These load drops did not occur directly after the load peak, but after some time when the ice and structure moved in the same direction (Figure 3 right). Once the structure moved faster than the ice for sufficient duration (negative relative velocity), the ice and structure lost contact. When we analyze the load time series in the frequency domain, we notice a large contribution of frequencies that

were significantly higher than the structural eigenfrequencies. Those frequencies were not observed in the frequency analysis of the structural displacement. Thus, either the structure or the measurement system acted as a low-pass filter. However, the structural frequencies were also found in the frequency domain of the ice load time signal, although here the frequencies were either higher or lower than the corresponding structural eigenfrequencies.

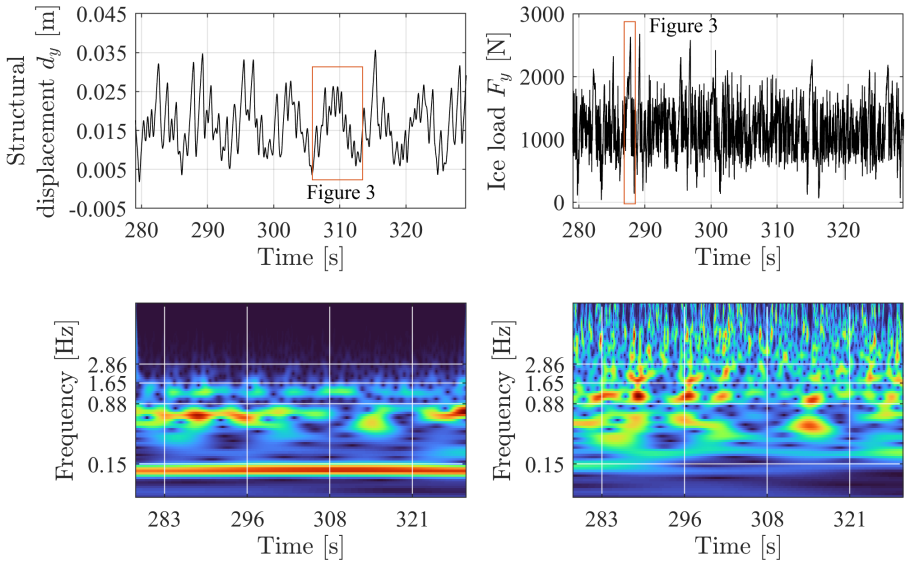

Figure 2. Measured structural displacement and ice load of case 1 for an ice drift speed of 30 mm s^{-1}. Orange boxes are shown in detail in Figure 3. In addition, corresponding continuous 1-D wavelet transformations based on the data resampled at 40 Hz are shown for the corresponding time series. Red color indicates a large value while blue indicate a low value.

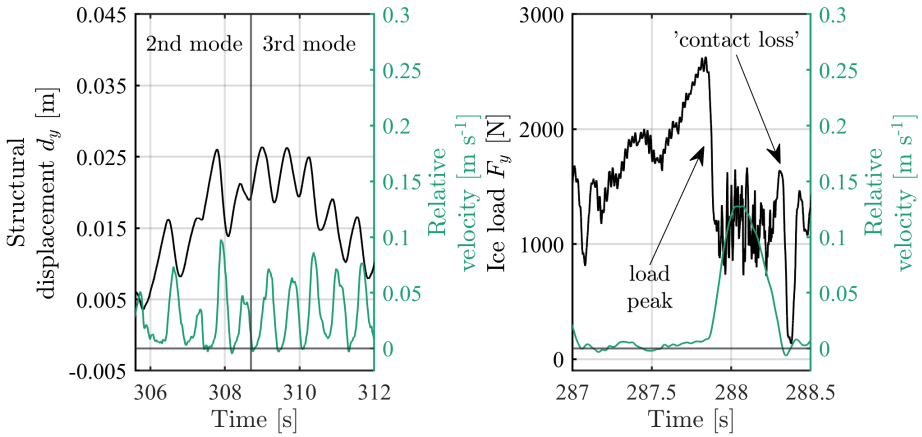

Figure 3. Detailed view of structural displacement and ice load from Figure 2. Left: Third mode vibrations were mainly present once the structure and ice moved in opposite direction. Right: The structure experienced load peaks and contact losses when vibrating.

Case 2 - Equalized mode shape amplitudes

For the next case, we equalized the mode shape amplitudes of the second and third eigenmode, while keeping the total structural stiffness and damping of the structure constant. Experimental

results for a test with an ice drift speed of 30 mm s^{-1} are shown in Figure 4. The measured structural displacement showed that the structure underwent oscillations of two frequencies mainly. The analysis in the frequency domain showed that the active frequencies were close to the second and third eigenfrequencies. However, we again observed that the oscillation frequencies were slightly below the structural eigenfrequencies. In comparison to the previous case, durations of single mode vibrations in this case were more continuous, and the structure tended to vibrate in the second eigenmode mainly. The first mode was not as present in this case as during the first case. The load time series of the second structural case showed similar results as for the first case. However, load peaks and contact losses occurred more regularly in this case. Although still recognizable, frequencies that are slightly smaller or larger than the natural structural frequencies were not as present as in the first case once we compared the load time series in the frequency domain.

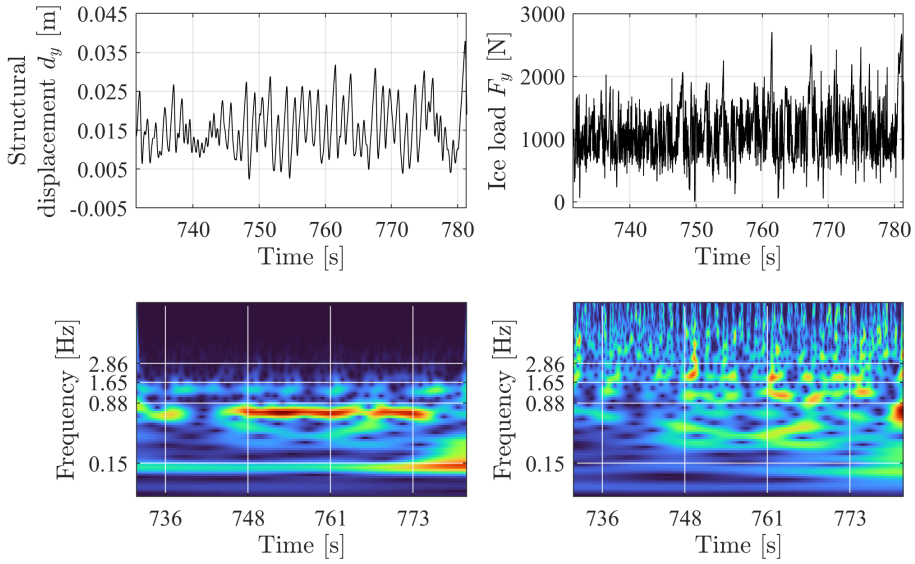

Figure 4. Measured structural displacement and ice load of case 2 for an ice drift speed of 30 mm s^{-1}. In addition, corresponding continuous 1-D wavelet transformations based on the data resampled at 40 Hz are shown for the corresponding time series. Red color indicates a large value while blue indicate a low value.

Case 3 – Large second mode shape amplitude

For the third case, we tuned the mode shape amplitudes of the third and second mode so that the magnitude of the second mode exceeded the mode shape amplitude of the third mode by a factor of 10 while keeping the total structural stiffness and damping of the structure constant. The measured structural displacement in Figure 5 for an ice drift speed of 50 mm s^{-1} shows the presence of oscillations of two frequencies mainly. The analysis in the frequency domain revealed that those were related to the first and second structural eigenfrequencies. Note that the measured frequencies were again slightly lower than the structural eigenfrequencies. The load time series shows peak loads and significant load reduction in phases of negative relative velocity. The frequency analysis showed that a frequency below or above the second eigenfrequency was present in the measured ice load signal. No significant contribution of the third eigenfrequency could be observed either in the displacement or in the load signal.

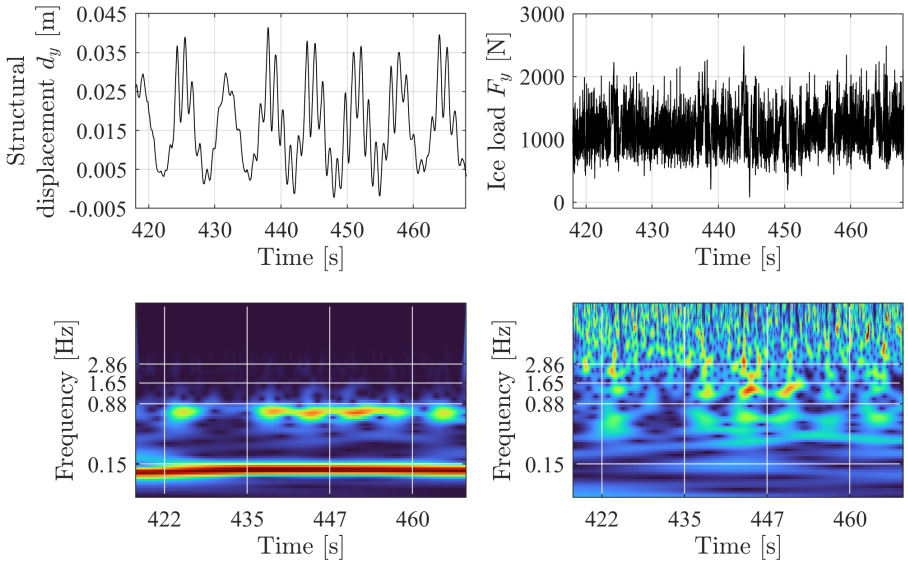

Figure 5. Measured structural displacement and ice load of case 3 for an ice drift speed of 50 mm s^{-1} In addition, corresponding continuous 1-D wavelet transformations based on the data resampled at 40 Hz are shown for the corresponding time series. Red color indicates a large value while blue indicate a low value.

Case 4 - Large third mode shape amplitude

Conversely to the third case, we tuned the mode shape amplitudes of the second and third mode, so that the third mode shape amplitude magnitude exceeded the mode shape amplitude of the second mode by a factor of 10, while keeping the waterline stiffness and damping of the structure constant. The measurement displacement in Figure 6 for a speed of 50 mm s^{-1} shows that the structure underwent oscillations of mainly two frequencies. The analysis of the time signal in the frequency domain showed that the frequencies measured are slightly lower than the first and third structural mode. While only slightly recognizable in the time series, the frequency analysis revealed that the structure even experienced single cycles of fourth mode vibrations. The load time series looked similar to that of the third case. However, the load time signal showed more load peak cycles due to the increased frequency of the lock-in phenomenon.

Summarizing the four different cases, we show the statistical measures of the ice load and structural displacement in Figure 7. For each case, we show the maximum, mean, and standard deviation. Note that we define the maximum value as the 99th percentile of the data. Figure 7 shows that case 3 and case 4 clearly resulted in an increase of maximum structural displacement and standard deviation, although a similar mean ice load was measured for both cases. Also, the maximum ice loads increased for case 3 and 4. For both observations, the effect increased with decreasing ice drift speed.

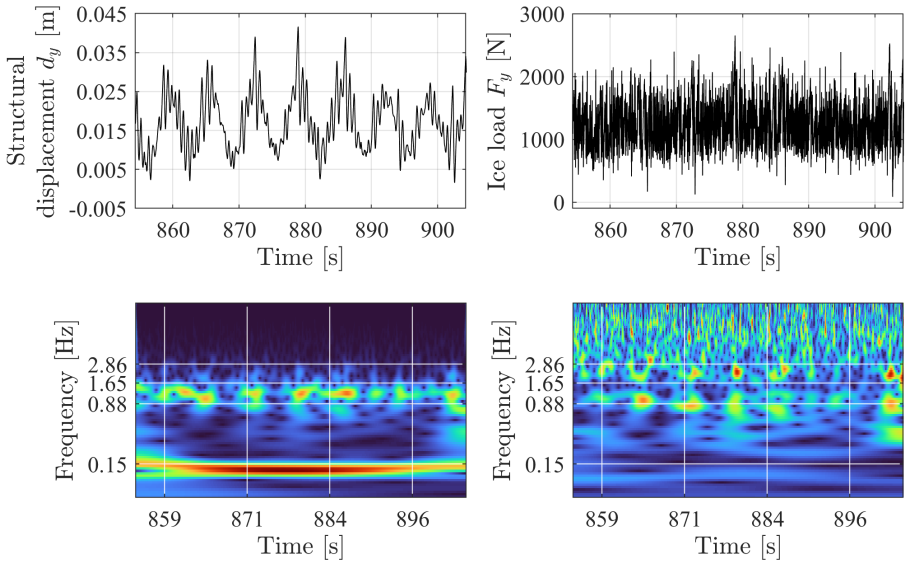

Figure 6. Measured structural displacement and ice load of case 4 for an ice drift speed of 50 mm s^{-1} In addition, corresponding continuous 1-D wavelet transformations based on the data resampled at 40 Hz are shown for the corresponding time series. Red color indicates a large value while blue indicate a low value.

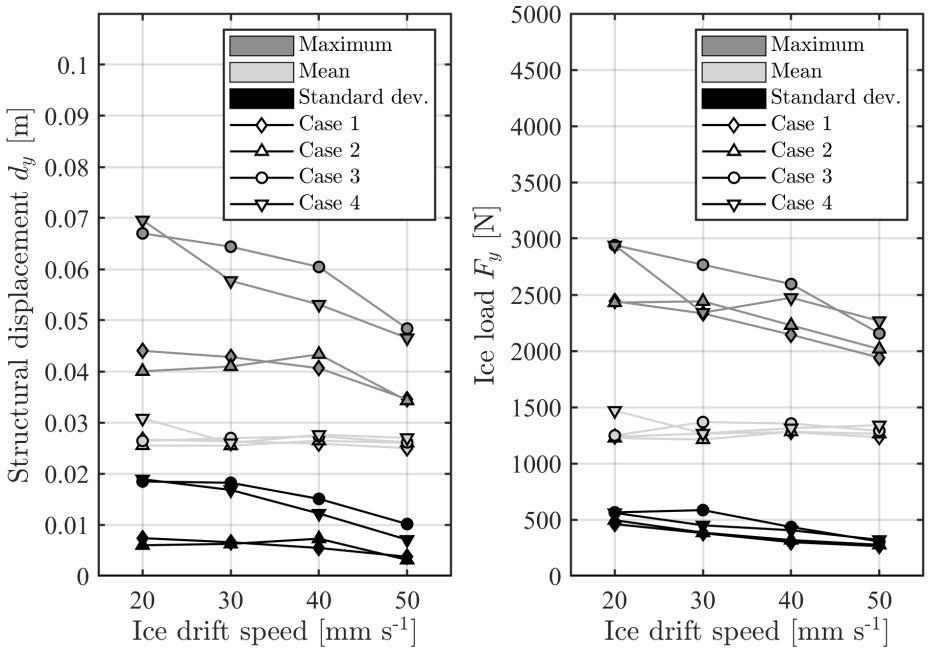

Figure 7. Statistical measures of the structural displacement and ice load for all cases.

Finally, we compare the measured structural displacement between three different configurations of constant ice drift speed and structural configurations in Figure 8. It can be seen that the fundamental mechanism behind the development of ice-induced vibrations is the same for all three configurations. For the lowest ice drift speed (left), the first mode became excited during phases of low relative velocities. Once the relative velocity increased when the structure crushed through the ice, the mode with the largest mode shape amplitude became

excited (second mode). When testing with a higher ice drift speed for case 1 (center), the second mode became excited during the phase of low relative velocity. Again, once the relative velocity increased when the structure crushed through the ice, the mode with the largest mode shape amplitude became excited (third mode). When testing with case 4 for a high ice drift speed (right), the structure vibrated in the third eigenfrequency during the phase of low relative velocity. Only in case 4 did the structure not follow the trend and did not experience sustained fourth mode vibrations during the phase of higher relative velocity as to be expected. Only a single cycle of fourth mode vibrations was observed. Figure 8 illustrates that ice-induced vibrations of multi-degree-of-freedom structures are highly dependent on the relative velocity between the ice and structure and thus on the superposition of higher mode oscillations with lower mode oscillations.

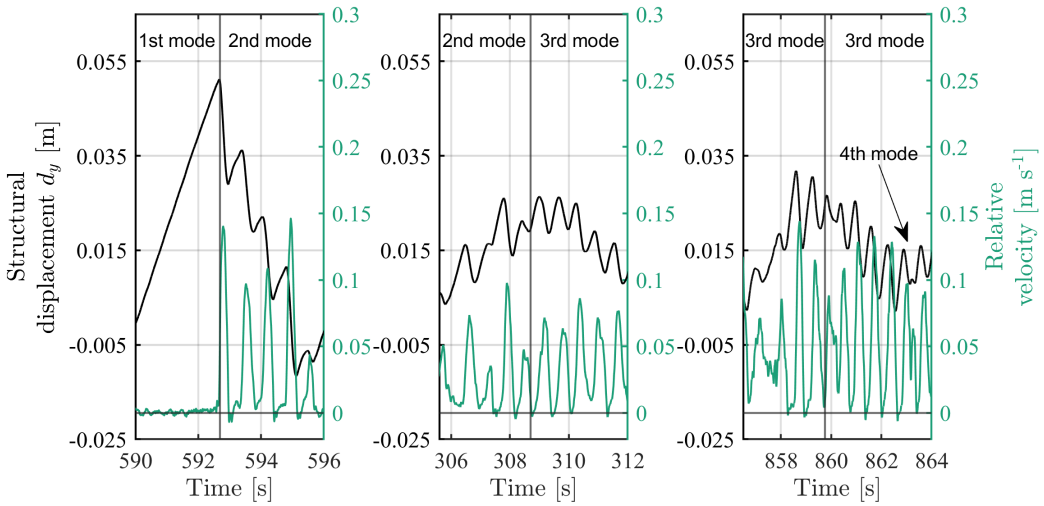

Figure 8. Left: Experimental results of case 4 for an ice drift speed of 20 mm s^{-1}. Center: Experimental results of case 1 for an ice drift speed of 30 mm s^{-1}. Right: Experimental results of case 4 for an ice drift speed of 50 mm s^{-1}.

After presenting the results of ice-induced vibrations experiments of four different structural configurations, we can summarize that:

- a frequency lock-in 'competition' between second and third mode vibrations occurred for the structural reference case (case 1). Once the mode shape amplitudes were equalized (case 2), the structure tended to undergo oscillations with a frequency close to the second eigenfrequency superposed on a first mode oscillation.
- the structure experienced sustained frequency lock-in vibrations, superposed on first mode oscillations, in a frequency corresponding to the mode shape amplitude of artificially high magnitude (case 3 & 4).
- increased maxima of the measured structural displacement and increased maxima and standard deviations of the measured ice load occurred once either the second or the third mode shape amplitude exceeded the other by a factor 10 (case 3 & 4).

Furthermore, we found that:

- all tested structures resulted in ice-induced vibrations of multiple structural frequencies, wherein frequencies of the measured structural displacement were slightly lower than

the natural eigenfrequencies, and frequencies within the ice load signal were either lower or higher than the natural eigenfrequencies.

- the case 3 and case 4 sustained ice-induced vibrations up to higher ice drift speeds, e.g., showing contributions of first mode structural vibrations up to higher ice drift speeds, which is why we had to show data for a higher ice drift speed for those cases.

DISCUSSION

Ice-structure coupling

Identified frequencies in the measured structural response were lower than the natural frequencies. Frequency analysis of the ice load time series showed frequencies at the lower and upper boundary of the natural eigenfrequency, and a clear absence of any natural frequency content. This observation showed that ice-structure interaction should consider the coupling between structure and ice. The ice either adds stiffness or mass to the dynamic system once coupled. Ice load signals recorded from Nord et al. (2013, 2015) indicated that the coupled frequencies were below the natural frequency as can be seen from Figure 4 and Figure 5 in their publications, respectively. However, we can only conclude here that the ice load explicitly did not show a contribution of the structural eigenfrequencies.

Higher mode vibrations

Reflecting the finding from Määttänen (1983), we agree that higher mode vibrations can be expected to occur when relatively higher ice drift speeds are tested. However, those higher modes do not necessarily become the dominant mode. Rather, the higher modes may superpose with first mode oscillations. We therefore agree with Nord et al. (2015) that during ice-structure interaction more than one mode of the structure can be excited. We further observed that ice-induced vibrations are not necessarily dominated by mode vibration of the lowest natural frequency, as described by Kärnä et al., (2003), but rather by the most critical combination of mode(s) shape amplitude(s) and relative velocity between ice and structure. When coupling an ice model to a structural model of an offshore wind turbine, Hendrikse (2017) also concluded that ice-induced vibrations are dominated by the mode shape amplitude. We can imagine that previous test campaigns (Määttänen, 1983; Kärnä et al., 2003; Määttänen et al., 2012) overestimated the frequency lock-in sensitivity of the first mode, as tested eigenfrequencies were too high. First mode oscillations in the range of our test cases changed the relative velocity between the ice and structure, thus initiating different modal vibrations of higher frequency at different time instances within a single first mode structural oscillation.

As we kept the total structural stiffness constant but changed solely the mass-normalized mode shape amplitude, we want to emphasize that observations presented are neither related to a change in stiffness nor change in frequency. For example, we noticed that case 3 and case 4 sustained first mode oscillations up to higher ice drift speeds, although solely the relation between second and third mode had been adjusted. We therefore can adjust the conclusion of Nord et al., (2015) in a way that it is the distribution of mass-normalized mode shape amplitudes of higher modes that shifts the transition speed from first to second (or third) mode vibrations. Further, we can confirm the observation of Nord, Määttänen and Øiseth, (2013) that the maximum ice load increases when the response has more than one major frequency component active and that the ice-induced load (standard deviation) and maximum displacement depends on the activated modes.

As the relative velocity between ice and structure can be expected to define the development of frequency lock-in vibrations (see Toyama et al. (1983)), a ‘constant’ carriage/indenter

velocity needs to be guaranteed during experiments (see Määttänen (1983)).

We expect that it is unlikely that a multi-degree-of-freedom structure (in a reasonable range of our investigated structures) will ever experience frequency lock-in a single frequency. This observation instigated Hammer et al. (2022) to replace frequency lock-in by multi-modal interaction with an indicator for the dominant mode for multi-degree-of-freedom structures. Finally, we can imagine that the idea of a dominant single mode vibration during frequency lock-in for a multi-degree-of-freedom structure originates from the choice of model ice tested. For example, Figure 5 of Hendrikse et al., (2022b), showed that tempered model ice more easily synchronizes with the structure and significantly enhances the development of frequency lock-in.

The presented results might motivate the investigation of the application range of a single mode semi-empirical vulnerability criterion (Määttänen, 1978), an analytical frequency lock-in assessment of offshore wind turbine monopiles (e.g. Seidel and Hendrikse (2018)), and numerical simulations of ice models coupled to multi-degree of freedom structures (Kärnä et al., 2010; Hendrikse, 2017; Hendrikse and Nord, 2019).

Limitations

We could not distinguish if the first structural mode vibrated because of the set of initial conditions or because of the set of tested parameters. Dedicated tests with longer test length could be conducted to improve these insights. However, the full time series indicated that the effect of transient vibrations could be neglectable. To investigate if our results could be generalized for higher structural modes, tests with structures consisting of higher structural modes could be conducted. However, such experiments could bring the complexity of data analysis to a point where distinction between oscillation of single structural modes is not possible.

CONCLUSIONS

To investigate the influence of a sole change of mode-shape amplitude on the development of frequency lock-in for multi-degree-of-freedom structures, small-scale experiments of a vertical structure in model ice were performed using a hybrid test method. Numerical models with exclusively-tuned mode shape amplitudes at the water level were implemented in a physical test setup to analyze the development of frequency lock-in higher structural modes. Higher mode oscillation could be controlled by a sole change of mass-normalized mode-shape amplitude, while keeping stiffness and damping constant. Ice-induced vibrations of multi-degree-of-freedom structures are highly dependent on the relative velocity between the ice and structure and thus on the superposition of higher mode oscillations with lower mode oscillations.

ACKNOWLEDGEMENTS

The authors thank the participating organizations in the SHIVER project: TU Delft, Siemens Gamesa Renewable Energy, and Aalto University, for supporting this work. The SHIVER project is co-financed by Siemens Gamesa Renewable Energy and TKI-Energy by the ‘Toeslag voor Topconsortia voor Kennis en Innovatie (TKI’s)’ of the Dutch Ministry of Economic Affairs and Climate Policy. We thank the crew of the Aalto ice tank: Otto Puolakka, Teemu Päivärinta, Lasse Turja and Sampo Hanhirova, for their help in preparation and installation of the setup and execution of tests. A special thanks goes to Cody C. Owen for providing valuable feedback and for proofreading of the document.

REFERENCES

Barker, A. et al. (2005) 'Ice loading on Danish wind turbines. Part 1: Dynamic model tests', *Cold Regions Science and Technology*, 41(1), pp. 1–23. Available at: https://doi.org/10.1016/j.coldregions.2004.05.002.

Cole, D.M. (2021) 'A constitutive model for sea ice: physical basis, formulations, examples and applications', in *Proceedings of the 26th International Conference on Port and Ocean Engineering under Arctic Conditions*. Moscow, Russia: POAC, pp. 1–12. Available at: http://www.poac.com/PapersOnline.html.

Hammer, T.C. et al. (2021) 'A 2D test setup for scaled real-time hybrid tests of dynamic ice-structure interaction', in *Proceedings of the 26th International Conference on Port and Ocean Engineering under Arctic Conditions*. Moscow, Russia: POAC, pp. 1–13. Available at: http://www.poac.com/PapersOnline.html.

Hammer, T.C. et al. (2022) 'Classification of ice-induced vibration regimes of offshore wind turbines', in *Proceedings of the ASME 2022 41st International Conference on Ocean, Offshore and Arctic Engineering*. Hamburg, Germany: OMAE, pp. 1–8. Available at: https://doi.org/https://doi.org/10.1115/OMAE2022-78972.

Hammer, T.C. and Hendrikse, H. (2023) 'Experimental study into the effect of wind-ice misalignment on the development of ice-induced vibrations of offshore wind turbines', *Engineering Structures*. Available at: https://doi.org/10.1016/j.engstruct.2023.116106.

Hammer, T.C., Willems, T. and Hendrikse, H. (2023) 'Dynamic ice loads for offshore wind support structure design', *Marine Structures*, pp. 1–19. Available at: https://doi.org/10.1016/j.marstruc.2022.103335.

Hendrikse, H. (2017) 'Ice-induced vibrations of vertically sided offshore structures'. Available at: https://doi.org/https://doi.org/10.4233/uuid:325ebcfb-f920-400c-8ef6-21b2305b6920.

Hendrikse, H., et al. (2022a) 'Experimental data from ice basin tests with vertically sided cylindrical structures', *Data in Brief*, 41, pp. 1–18. Available at: https://doi.org/10.1016/j.dib.2022.107877.

Hendrikse, H., et al. (2022b) 'Ice basin tests for ice-induced vibrations of offshore structures in the SHIVER project', in *Proceedings of the ASME 2022 41st International Conference on Ocean, Offshore and Arctic Engineering*. Hamburg, Germany: OMAE, pp. 1–9. Available at: https://doi.org/10.1115/OMAE2022-78507.

Hendrikse, H. and Nord, T.S. (2019) 'Dynamic response of an offshore structure interacting with an ice floe failing in crushing', *Marine Structures*, 65, pp. 271–290. Available at: https://doi.org/10.1016/j.marstruc.2019.01.012.

Hendrikse, H., Ziemer, G. and Owen, C.C. (2018) 'Experimental validation of a model for prediction of dynamic ice-structure interaction', *Cold Regions Science and Technology*, 151, pp. 345–358. Available at: https://doi.org/10.1016/j.coldregions.2018.04.003.

Huang, Y., Shi, Q. and Song, A. (2007) 'Model test study of the interaction between ice and a compliant vertical narrow structure', *Cold Regions Science and Technology*, 49(2), pp. 151–160. Available at: https://doi.org/10.1016/j.coldregions.2007.01.004.

International Towing Tank Conference (2014) 'Test Methods for Model Ice Properties', in *Proceedings of the 27th International Towing Tank Conference*. Copenhagen, Denmark: pp.1–19

Kärnä, T. et al. (2003) 'Tests on dynamic ice-structure interaction', in *Proceedings of the 22nd International Conference on Offshore Mechanics and Arctic Engineering*. Cancún, Mexico: OMAE, pp. 1–7. Available at: https://asmedigitalcollection.asme.org/OMAE/proceedings-abstract/OMAE2003/36835/823/298517.

Kärnä, T. et al. (2010) 'Simulation of multi-modal vibrations due to ice actions', in *Proceedings of the 20th IAHR International Symposium on Ice*. Lathi, Finland: IAHR, pp. 1–12

Määttänen, M. (1978) 'On conditions for the rise of self-excited autonomous oscillations in slender marine piles', *Winter Navigation Reseach Board*, (Research Report No 25), pp. 1–101.

Määttänen, M. (1983) *Dynamic ice-structure interaction during continuous crushing*. U.S. Army Cold Regions Research and Engineering Laboratory. Hanover, New Hampshire, USA: CRREL: pp 1–48. Available at: https://apps.dtic.mil/docs/citations/ADA126349.

Määttänen, M. et al. (2012) 'Novel ice induced vibration testing in a large-scale facility: Deciphering ice induced vibrations, part 1', in *Proceedings of the 21st IAHR International Symposium on Ice*. Dalian, China: IAHR, pp. 946–958.

Nord, T.S. et al. (2015) 'Laboratory experiments to study ice-induced vibrations of scaled model structures during their interaction with level ice at different ice velocities', *Cold Regions Science and Technology*, 119, pp. 1–15. Available at: https://doi.org/10.1016/j.coldregions.2015.06.017.

Nord, T.S., Määttänen, M. and Øiseth, O. (2013) 'Frequency domain force identification in ice-structure interaction', in *Proceedings of the 22nd International Conference on Port and Ocean Engineering under Arctic Conditions*. Espoo/Helsinki, Finalnd: POAC, pp. 1–10. Available at: http://www.poac.com/PapersOnline.html.

Palmer, A. and Dempsey, J. (2009) 'Model tests in ice', in *Proceedings of the 20th International Conference on Port and Ocean Engineering under Arctic Conditions*. Luleå, Sweden: POAC, pp. 1–10. Available at: http://www.poac.com/PapersOnline.html.

Seidel, M. and Hendrikse, H. (2018) 'Analytical assessment of sea ice-induced frequency lock-in for offshore wind turbine monopiles', *Marine Structures*, 60, pp. 87–100. Available at: https://doi.org/10.1016/J.MARSTRUC.2018.02.003.

Sodhi, D.S. (2001) 'Crushing failure during ice-structure interaction', *Engineering Fracture Mechanics*, 68(17–18), pp. 1889–1921. Available at: https://doi.org/10.1016/S0013-7944(01)00038-8.

Tian, Y., Huang, Y. and Li, W. (2019) 'Experimental Investigations on Ice Induced Vibrations of a Monopile-type Offshore Wind Turbine in Bohai Sea', in *Proceedings of the 29th International Ocean and Polar Engineering Conference*. Honolulu, Hawaii, USA: ISOPE, pp. 327–334.

Toyama, Y. et al. (1983) 'Model tests on ice-induced self-excited vibration of cylindrical structures', in *Proceedings of the International Conference on Port and Ocean Engineering under Arctic Conditions*. Helsinki, Finland: POAC, pp. 834–844. Available at: http://www.poac.com/PapersOnline.html.